

Chemical Abundances of the Secondary Star in the Black Hole X-ray Binary XTE J1118+480

Jonay I. González Hernández^{1,2,3}, Rafael Rebolo^{3,4}, Garik Israelian³, Alexei V. Filippenko⁵,
Ryan Chornock⁵, Nozomu Tominaga⁶, Hideyuki Umeda⁶, and Ken'ichi Nomoto^{6,7,8}

ABSTRACT

Following the recent abundance measurements of Mg, Al, Ca, Fe, and Ni in the black hole X-ray binary XTE J1118+480 using medium-resolution Keck II/ESI spectra of the secondary star (González Hernández et al. 2006), we perform a detailed abundance analysis including the abundances of Si and Ti. These element abundances, higher than solar, indicate that the black hole in this system formed in a supernova event, whose nucleosynthetic products could pollute the atmosphere of the secondary star, providing clues on the possible formation region of the system, either Galactic halo, thick disk, or thin disk. We explore a grid of explosion models with different He core masses, metallicities, and geometries. Metal-poor models associated with a formation scenario in the Galactic halo provide unacceptable fits to the observed abundances, allowing us to reject a halo origin for this X-ray binary. The thick-disk scenario produces better fits, although they require substantial fallback and very efficient mixing processes between the inner layers of the explosion and the ejecta, making quite unlikely an origin in the thick disk. The best agreement between the model predictions and the observed abundances is obtained for metal-rich progenitor models. In particular, non-spherically symmetric models are able to explain, without strong assumptions of extensive fallback and mixing, the observed abundances. Moreover, asymmetric mass ejection in a supernova explosion could account for the required impulse necessary to launch the system from its formation region in the Galactic thin disk to its current halo orbit.

Subject headings: black holes: physics — stars: abundances — stars: evolution — stars: individual (XTE J1118+480) — supernovae: general — X-rays: binaries

¹Observatoire de Paris-Meudon, GEPI, 5 place Jules Janssen, 92195 Meudon Cedex, France; Jonay.Gonzalez-Hernandez@obspm.fr

²CIFIST Marie Curie Excellence Team

³Instituto de Astrofísica de Canarias, E-38205 La Laguna, Tenerife, Spain; rrl@iac.es, gil@iac.es

⁴Consejo Superior de Investigaciones Científicas, Spain.

⁵Department of Astronomy, University of California, Berkeley, CA 94720-3411, USA;

alex@astro.berkeley.edu,
rchornock@astro.berkeley.edu

⁶Department of Astronomy, School of Science, University of Tokyo, Bunkyo-ku, Tokyo 113-0033, Japan; tominaga@astron.s.u-tokyo.ac.jp, umeda@astron.s.u-tokyo.ac.jp, nomoto@astron.s.u-tokyo.ac.jp

⁷Research Center for the Early Universe, School of Science, University of Tokyo, Bunkyo-ku, Tokyo 113-0033, Japan.

⁸Institute for the Physics and Mathematics of the

1. Introduction

The low-mass X-ray binary XTE J1118+480 is the first identified black hole moving in Galactic halo regions (Wagner et al. 2001; Mirabel et al. 2001). Since it was discovered during a faint outburst on UT 2000 March 29 (Remillard et al. 2000), it has been intensively studied in both the X-ray and optical spectral regions. During the decay of the outburst, McClintock et al. (2001) and Wagner et al. (2001) determined the radial-velocity curve of the companion star, yielding a mass function $f(M) \approx 6 M_\odot$. The companion star was classified as a late-type main-sequence star with a mass of $0.1\text{--}0.5 M_\odot$ (Wagner et al. 2001).

By modelling the light curve, McClintock et al. (2001) derived a lower limit to the orbital inclination, $i \gtrsim 55^\circ$, and consequently an upper limit to the black hole mass of $M_{\text{BH}} \lesssim 10 M_\odot$. Additional evidence for a high inclination ($i \gtrsim 60^\circ$) comes from measurements of tidal distortion (Frontera et al. 2001), whereas the lack of dips or eclipses for a Roche-lobe filling secondary yields upper limits of $i \gtrsim 80^\circ$ and $M_{\text{BH}} \gtrsim 7.1 M_\odot$. Later, Gelino et al. (2006) derived an orbital inclination of $68^\circ \pm 2^\circ$, by modeling the optical and infrared ellipsoidal light curves of the system in quiescence. This value of the inclination allowed them to better constrain the black hole mass at $M_{\text{BH}} = 8.53 \pm 0.60 M_\odot$.

The system is placed in the Galactic halo, with an extraordinarily high Galactic latitude ($b \approx 62.3^\circ$), and a height of ~ 1.6 kpc above the Galactic plane, according to its distance of 1.85 ± 0.36 kpc (Wagner et al. 2001). This appears surprising since all other black hole binaries are located in the Galactic disk. An accurate measurement of its proper motion coupled with its distance provides space-velocity

components (U , V) which seem consistent with those of some old halo globular clusters (Mirabel et al. 2001). This opened the possibility that the system originated in the Galactic halo, and therefore, that the black hole could be either the remnant of a supernova (SN) in the very early Galaxy or the result of direct collapse of an ancient massive star. However, the galactocentric orbit crossed the Galactic plane many times in the past, and the system could have formed in the Galactic disk and been launched into its present orbit as a consequence of the “kick” imparted during the SN explosion of a massive star (Gualandris et al. 2005). Recent observations with the 10-m Keck II telescope revealed that the secondary star has a supersolar surface metallicity ($[\text{Fe}/\text{H}] = 0.2 \pm 0.2$, González Hernández et al. 2006), confirming the origin of the black hole in a SN event. Thus, if the system originated in the Galactic halo, the element abundances of the secondary star must have been enriched by a factor of 5–25 depending on whether its initial metallicity resembled a thick-disk star or a halo star.

Element abundances of secondary stars of X-ray binaries have been studied for the systems Nova Scorpii 1994 (Israelian et al. 1999; González Hernández et al. 2007), A0620–00 (González Hernández et al. 2004), Centaurus X-4 (González Hernández et al. 2005), XTE J1118+480 (González Hernández et al. 2006, hereafter Paper I), and V4641 Sagittarii (Orosz et al. 2001; Sadakane et al. 2006). All of these X-ray binaries show metallicities close to solar independent of their location with respect to the Galactic plane, and possible scenarios of pollution from a SN or hypernova have been discussed. In this paper, we compare in detail different scenarios of the possible enrichment of the secondary star from SN yields, providing conclusions on the formation region (Galactic halo, thick disk, or thin disk) of this halo black hole X-ray binary.

Universe, University of Tokyo, Kashiwa, Chiba 277-8582, Japan.

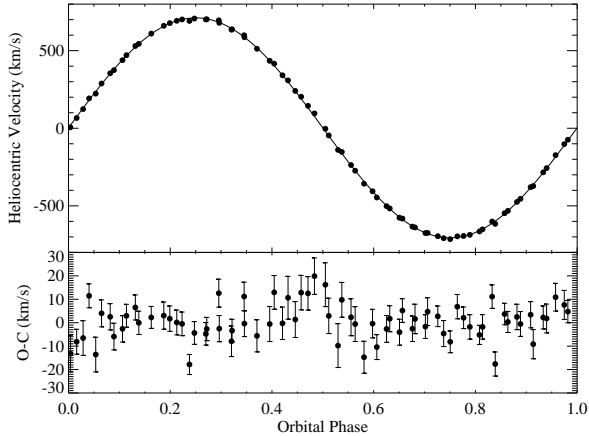


Fig. 1.— Radial velocities of XTE J1118+480 folded on the orbital solution of the data, together with the best-fitting sinusoid. Individual velocity uncertainties are $\leq 7 \text{ km s}^{-1}$ and are not plotted because they are always smaller than the symbol size. The bottom panel shows the residuals of the fit.

2. Observations

As already reported in Paper I, we obtained 74 medium-resolution spectra of the black hole X-ray binary XTE J1118+480, in quiescence, with the Echelle Spectrograph and Imager (ESI; Sheinis et al. 2002) at the 10-m Keck II telescope on UT 14 February 2004. The data covered the spectral range 4000–9000 Å at a resolving power $\lambda/\Delta\lambda \approx 6,000$. We also observed ten template stars with spectral types in the range K0V–M2V with the same instrument and spectral configuration. The exposure time was fixed at 300 s to minimize the effects of orbital smearing which, for the orbital parameters of XTE J1118+480, is in the range 0.6–26.6 km s^{-1} , smaller than the instrumental resolution of 50 km s^{-1} . All of the spectra were reduced in a standard manner.

3. Revised Orbital Parameters

We extracted the radial velocities by cross-correlating each target spectrum with the

spectrum of a K5V template star, using the software MOLLY developed by T. R. Marsh. We fitted these data with a sine wave using a χ^2 method providing the following orbital solution (see Fig. 1): $\gamma = 2.7 \pm 1.1 \text{ km s}^{-1}$, $K_2 = 708.8 \pm 1.4 \text{ km s}^{-1}$, $P = 0.16995 \pm 0.00012 \text{ d}$, and $T_0 = 2,453,049.93346 \pm 0.00007 \text{ d}$, where T_0 is defined as the corresponding time of the closest inferior conjunction of the companion star, and the quoted uncertainties are 1σ . This orbital period, P , and the velocity amplitude of the orbital motion of the secondary star, K_2 , lead to a mass function of $f(M) = 6.27 \pm 0.04 M_\odot$, consistent with (but more precise than) previous results (McClintock et al. 2001; Wagner et al. 2001; Torres et al. 2004).

The derived radial velocity of the center of mass of the system agrees somewhat (at the 3σ level) with previous studies ($\gamma = +26 \pm 17 \text{ km s}^{-1}$, McClintock et al. 2001; $\gamma = -15 \pm 10 \text{ km s}^{-1}$, Wagner et al. 2001; $\gamma = +16 \pm 6 \text{ km s}^{-1}$, Torres et al. 2004). Note that our medium-resolution data have a factor of ≥ 4 higher spectral resolution than the data these authors used. We estimate the uncertainty in our individual radial-velocity measurements of typically 6 km s^{-1} (see Fig. 1).

3.1. Secondary Spectrum

The individual spectra were corrected for their radial velocity and combined in order to improve the signal-to-noise ratio (S/N). After binning in wavelength in steps of 0.3 Å, the final spectrum had $S/N \approx 80$ in the continuum in the red spectral region. This spectrum, displayed in Fig. 2, was compared with ten template stars having spectral types K0V to M2V. The best fit shows a K5V star rather than the later spectral types (K7/8V or even M) suggested in previous studies (Wagner et al. 2001; Torres et al. 2004).

We should remark that the spectrum of the secondary star in this system and the spectra

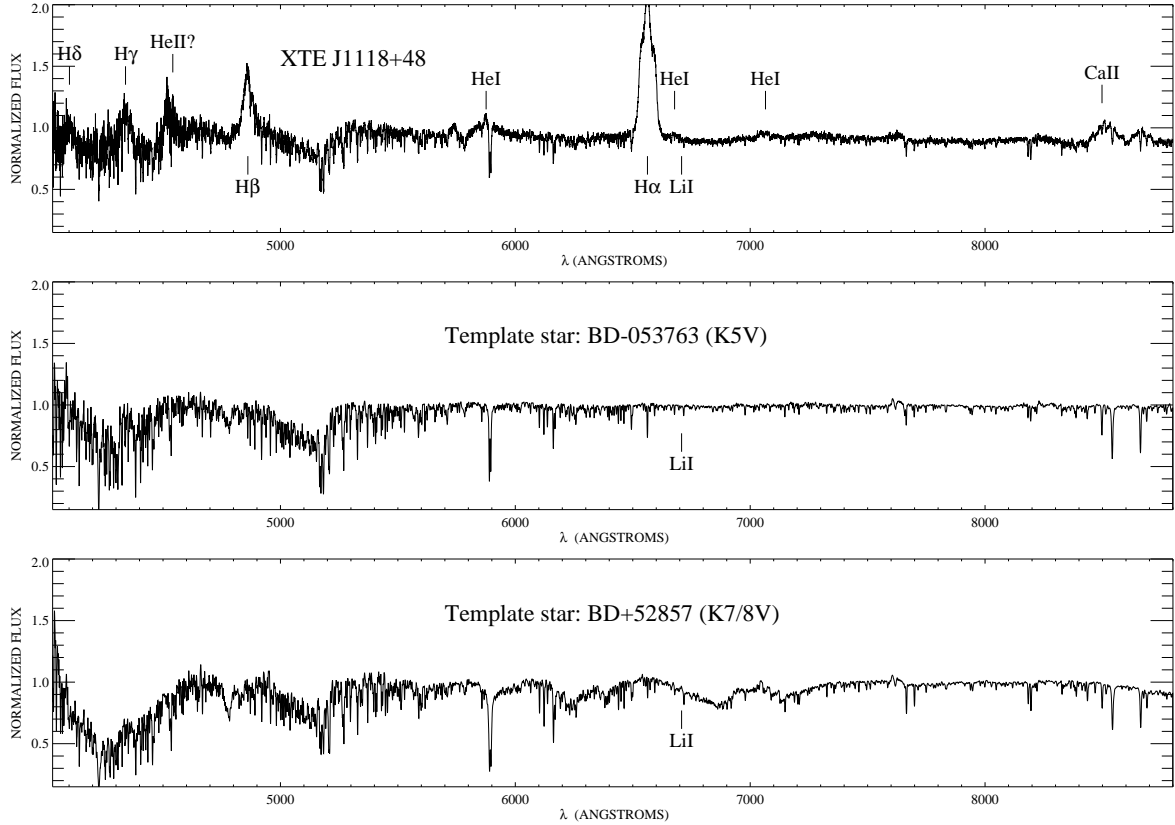


Fig. 2.— Observed spectrum of the secondary star of XTE J1118+480 (top panel) and of two properly broadened templates (BD−053763, middle panel; BD+52857, bottom panel).

of the template stars were normalized using the same procedure. The continuum was fitted with a low-order spline, in order to avoid the smoothing of possible existing broad TiO bands. Following Marsh et al. (1994), we computed the optimal value of $v \sin i$ by subtracting broadened versions of the K5V template (in steps of 1 km s^{-1}) and minimizing the residual. We used a spherical rotational profile with linearized limb-darkening $\epsilon = 0.8$ (Al-Naimiy 1978) due to the spectral type K of the secondary star. The best fit corresponds to $v \sin i = 100^{+3}_{-11} \text{ km s}^{-1}$, where the uncertainties have been derived by assuming extreme cases for $\epsilon = 0 - 1$. Our derived rotational velocity, combined with our value of the velocity amplitude, K_2 , implies a binary

mass ratio $q = 0.027 \pm 0.009$, in agreement with previous results (Torres et al. 2004, and references therein).

4. Chemical Analysis

4.1. Stellar Parameters

The normalized spectra of X-ray transients, although observed in quiescence, show apparently weaker stellar lines of the secondary star due to the veiling caused by the accretion disk. The veiling from the accretion disk was estimated to be $\sim 65\% \pm 8\%$ in the spectral range 5800–6400 Å in December 2000 and January 2001, and $\sim 40\% \pm 10\%$ in January 2003, by performing standard optimal subtraction techniques with K5V–M0V template stars.

TABLE 1
RANGES AND STEPS OF MODEL PARAMETERS

| Parameter | Range | Step |
|---------------------------|---------------------------|----------|
| T_{eff} | 3500 \rightarrow 5000 K | 100 K |
| $\log[g/(\text{cm s}^2)]$ | 4 \rightarrow 5 | 0.1 |
| [Fe/H] | -1.5 \rightarrow 1 | 0.1 |
| f_{4500} | 0 \rightarrow 2 | 0.1 |
| m_0 | 0 \rightarrow -0.00091 | -0.00010 |

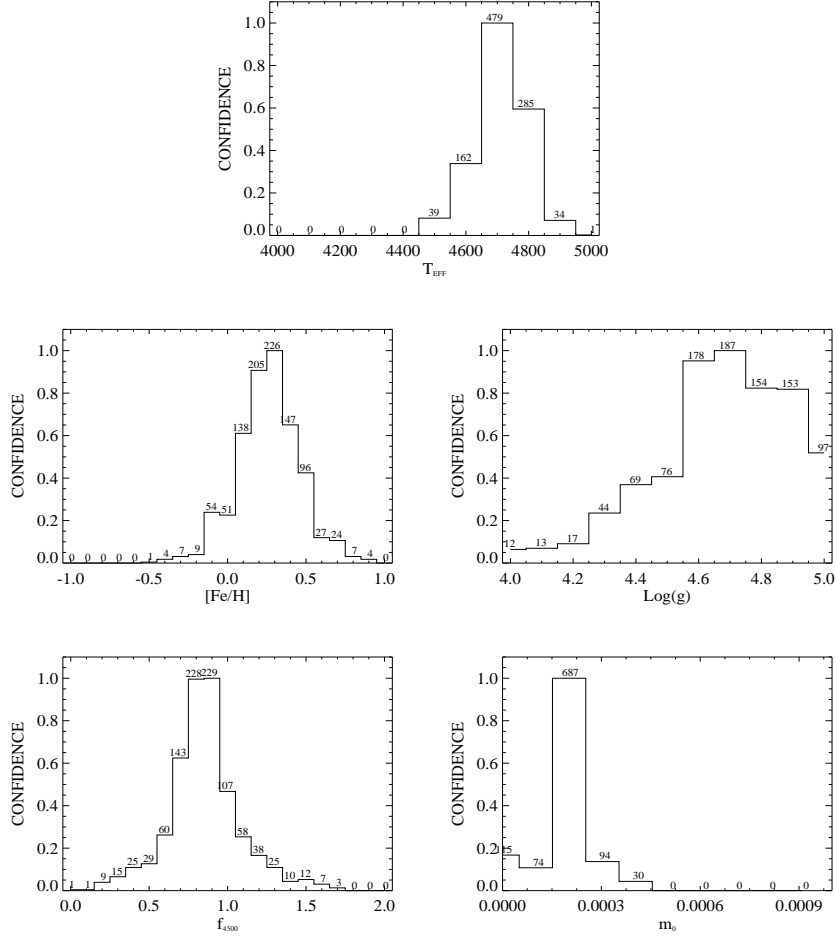


Fig. 3.— Distributions obtained for each parameter using Monte Carlo simulations. The labels at the top of each bin indicate the number of simulations consistent with the bin value. The total number of simulations was 1000.

As shown in Paper I, we tried to infer the stellar parameters, T_{eff} and $\log g$, and the metallicity [Fe/H], of the secondary star taking into account the veiling from the accretion disk, defined as a linear function of wave-

length and thus described with two additional parameters, the veiling at 4500 Å, $f_{4500} = F_{\text{disk}}^{4500}/F_{\text{sec}}^{4500}$, and the slope, m_0 . Note that the total flux is defined as $F_{\text{total}} = F_{\text{disk}} + F_{\text{sec}}$, where F_{disk} and F_{sec} are the flux contribu-

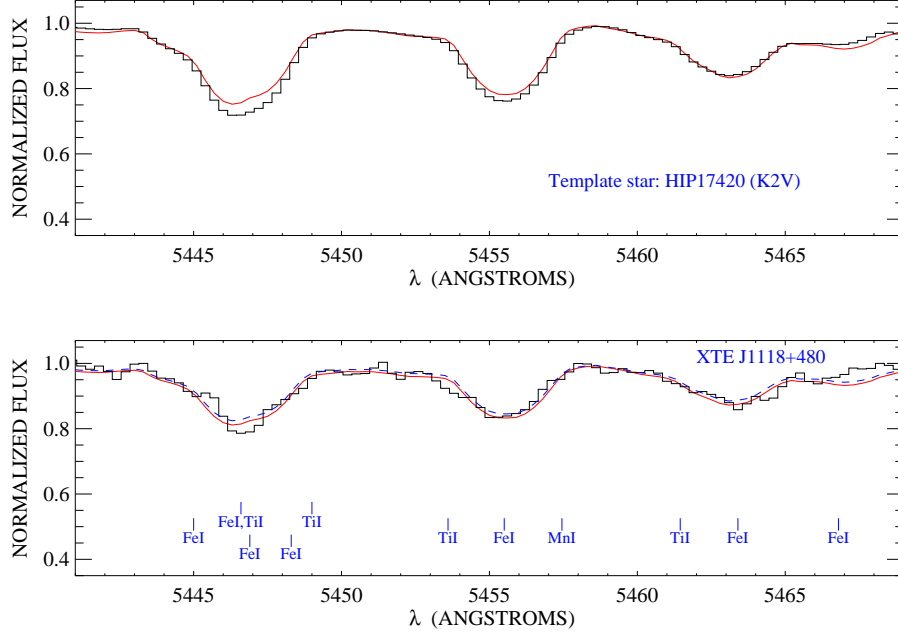


Fig. 4.— Best synthetic spectral fits to the Keck/ESI spectrum of the secondary star in the XTE J1118+480 system (bottom panel) and the same for a template star (properly broadened) shown for comparison (top panel). Synthetic spectra are computed for solar abundances (dashed line) and best-fit abundances (solid line).

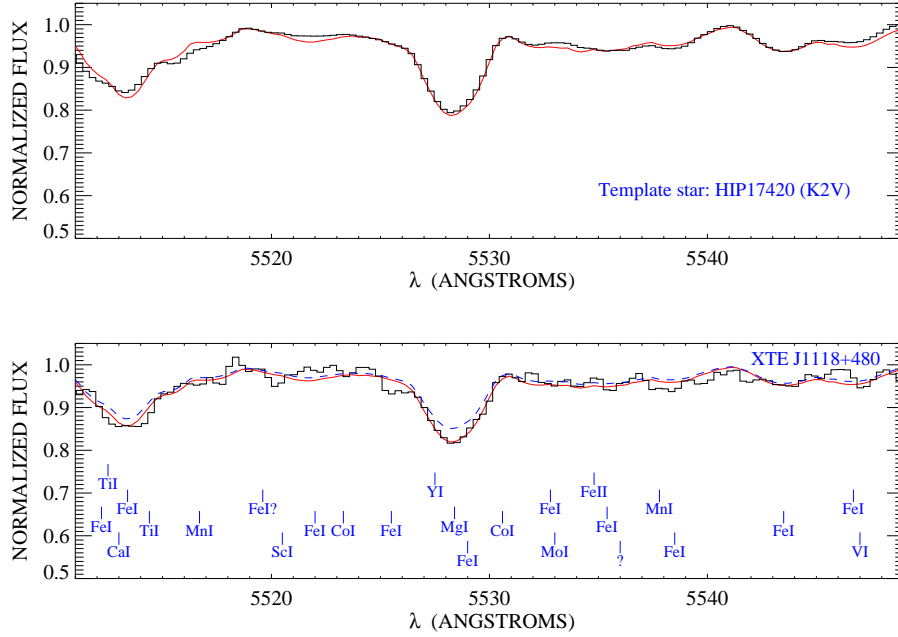


Fig. 5.— The same as in Fig. 4, but for the spectral range 5510–5550 Å.

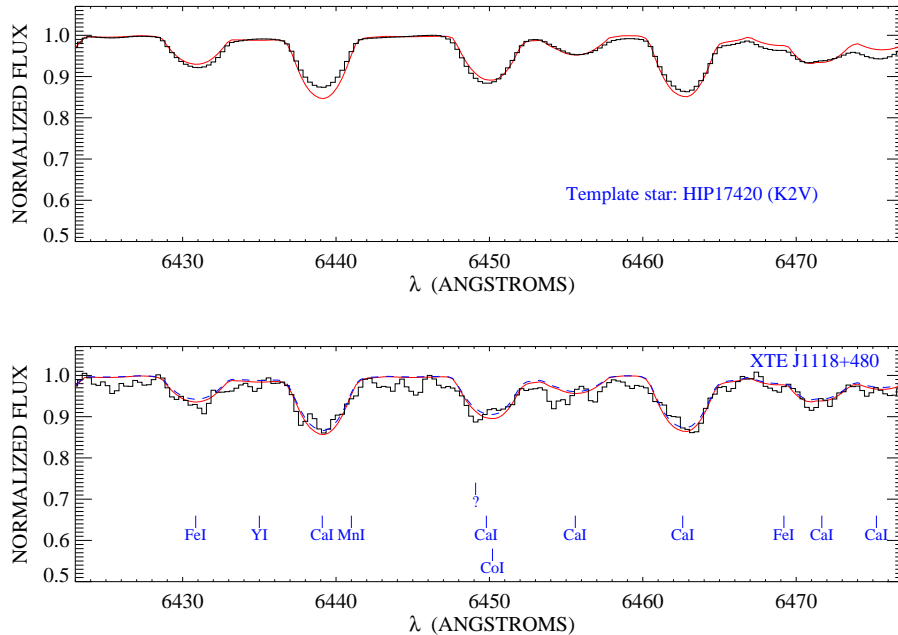


Fig. 6.— The same as in Fig. 4, but for the spectral range 6420–6480 Å.

tions of the disk and the continuum of the secondary star, respectively. This procedure involves a χ^2 minimization routine which compares several features of the stellar spectrum with a grid of synthetic spectra computed using the LTE code MOOG (Snedden 1973). We used a grid of LTE model atmospheres (Kurucz 1993) and atomic line data from the Vienna Atomic Line Database (VALD, Piskunov 1995). The oscillator strengths of relevant lines were adjusted until they reproduced the solar atlas (Kurucz et al. 1984) with solar abundances (Grevesse et al. 1996). The changes we applied to the $\log gf$ values taken from the VALD database were $\Delta \log gf \lesssim 0.2$ dex.

We selected nine spectral features containing in total 30 lines of Fe I and 8 lines of Ca I with excitation potentials between 1 and 5 eV. The five free parameters were varied in the ranges given in Table 1. For each given iron abundance in the range $[\text{Fe}/\text{H}] < 0$, the Ca

abundance was fixed according to the Galactic trend of Ca (Bensby et al. 2005), while for $[\text{Fe}/\text{H}] > 0$, we assumed $[\text{Ca}/\text{Fe}] = 0$. A rotational broadening of 100 km s^{-1} and a limb darkening $\epsilon = 0.8$ were adopted. The microturbulence, ξ , was computed using an experimental expression as a function of effective temperature and surface gravity (Allende Prieto et al. 2004).

The result, already presented in Paper I, provides as most likely values $T_{\text{eff}} = 4700 \pm 100 \text{ K}$, $\log[g/\text{cm s}^2] = 4.6 \pm 0.3$, $[\text{Fe}/\text{H}] = 0.18 \pm 0.17$, $f_{4500} = 0.85 \pm 0.20$, and $m_0 = -0.0002 \pm 0.0001$. The 1σ uncertainties of the five free parameters were determined using 1000 realizations whose corresponding histograms are displayed in Fig. 3.

The stellar parameters derived, especially the effective temperature, could provide important implications on the Gelino et al. (2006) determination of the orbital inclination of the system ($i \approx 68^\circ$). These authors mod-

TABLE 2
ABUNDANCE UNCERTAINTIES IN XTE J1118+480

| Element | $[X/H]_{\text{LTE}}^{\text{a}}$ | Δ_{σ} | $\Delta_{T_{\text{eff}}}$ | $\Delta_{\log g}$ | Δ_{veil} | $\Delta_{\text{tot}}^{\text{b}}$ | $n_{\text{lines}}^{\text{c}}$ |
|-----------------|---------------------------------|-------------------|---------------------------|-------------------|------------------------|----------------------------------|-------------------------------|
| Mg | 0.35 | 0.12 | 0 | -0.10 | 0.20 | 0.25 | 1 |
| Al | 0.60 | 0.12 | 0.05 | 0 | 0.15 | 0.20 | 1 |
| Si | 0.37 | 0.03 | -0.07 | 0.07 | 0.18 | 0.21 | 2 |
| Ca | 0.15 | 0.03 | 0.13 | -0.16 | 0.11 | 0.23 | 5 |
| Ti | 0.32 | 0.18 | 0.12 | -0.03 | 0.14 | 0.26 | 3 |
| Fe | 0.18 | 0.08 | 0.06 | 0.04 | 0.13 | 0.17 | 5 |
| Ni | 0.30 | 0 | 0.10 | 0.12 | 0.14 | 0.21 | 2 |
| Li ^d | 1.78 | 0.12 | 0.15 | 0.05 | 0.15 | 0.25 | 1 |

^aElement abundances of the secondary star (calculated assuming LTE) are $[X/H] = \log[N(X)/N(H)]_{\text{star}} - \log[N(X)/N(H)]_{\text{Sun}}$, where $N(X)$ is the number density of atoms. Uncertainties, $\Delta[X/H]$, are at the 1σ level and take into account the uncertainties in the stellar and veiling parameters.

^bThe total error was estimated as $\Delta_{\text{tot}} = \sqrt{\Delta_{\sigma}^2 + \Delta_{T_{\text{eff}}}^2 + \Delta_{\log g}^2 + \Delta_{\text{veil}}^2}$.

^cNumber of features analyzed for each element.

^dLi abundance is expressed as $\log \epsilon(\text{Li})_{\text{NLTE}} = \log[N(\text{Li})/N(\text{H})]_{\text{NLTE}} + 12$.

NOTE.—The uncertainties from the dispersion of the best fits to different features, Δ_{σ} , are estimated using the following formula: $\Delta_{\sigma} = \sigma/\sqrt{N}$, where σ is the standard deviation of the measurements.

eled the optical and infrared (IR) ellipsoidal light curves of XTE J1118+480 in quiescence, assuming a K7V spectral type ($T_{\text{eff}} \approx 4250$ K) for the secondary star. However, our spectroscopic value ($T_{\text{eff}} \approx 4700$ K) would require more contribution of the flux from the accretion disk in the K band. Gelino et al. (2001) derived an inclination of $i \approx 41^\circ$, yielding a black hole mass of $M_{\text{BH}} \approx 11 M_{\odot}$ for the A0620-00 system, by adopting $T_{\text{eff}} \approx 4600$ K, which is 300 K lower than the spectroscopic value reported by González Hernández et al. (2004). Hynes et al. (2005) suggested that this different effective temperature of the secondary star in A0620-00 would require a larger disk contribution in the K band, and therefore a higher inclination. In fact, Gelino et al. (2001) commented that if the K -band disk veiling as high as 50% of the total flux, the derived inclination would increase to 60° . The black hole mass would

then drop to $M_{\text{BH}} \approx 5 M_{\odot}$. Although this is an extreme case, milder IR veiling could still have a substantial impact on the derived black hole mass. Similarly, the black hole mass in XTE J1118+480 might be significantly affected when using our value of the effective temperature.

4.2. Stellar Abundances

We inspected several spectral regions in the observed Keck/ESI spectrum of the secondary star, searching for suitable lines for a detailed chemical analysis. Using the derived stellar parameters, we first determined the Fe abundance by comparing synthetic spectra with each individual feature in the ESI spectrum (see Table 2). In Fig. 4 (here) and Fig. 1 of Paper I, we display some of the spectral regions analyzed to obtain the Fe abundance. This figure also shows the best synthetic spectral fit to the observed spectrum of a template

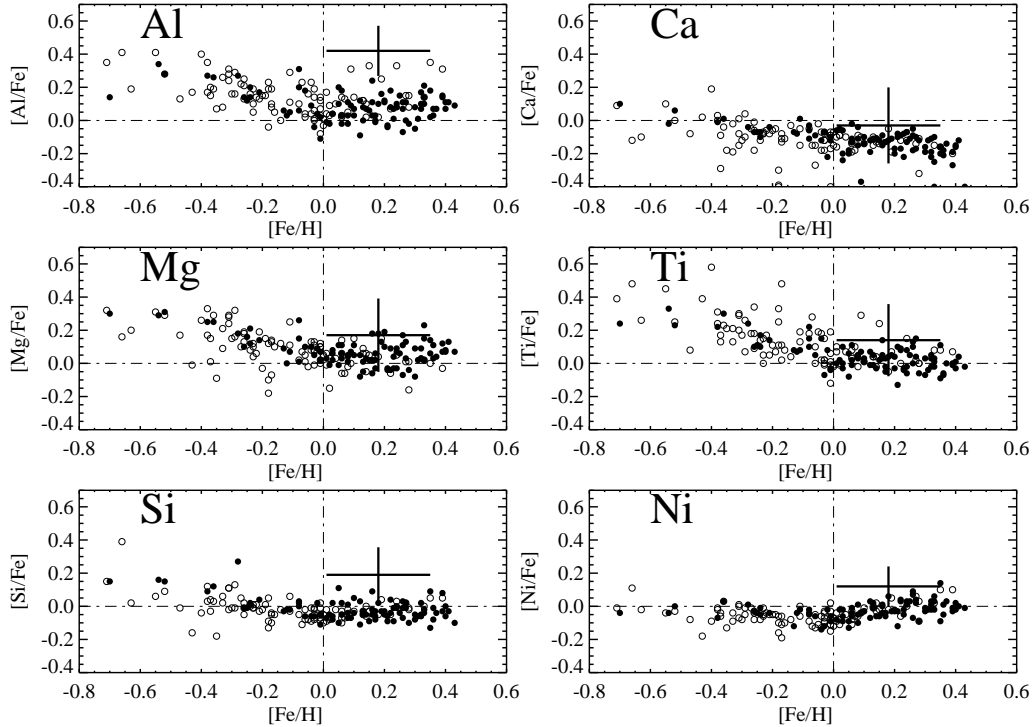


Fig. 7.— Abundance ratios of the secondary star in XTE J1118+480 (blue wide cross) in comparison with the abundances of G and K metal-rich dwarf stars. Galactic trends were taken from Gilli et al. (2006). The size of the cross indicates the uncertainty. Filled and empty circles correspond to abundances for exoplanet host stars and stars without known exoplanet companions, respectively. The dashed-dotted lines indicate solar abundance values.

star (HIP 17420 with $T_{\text{eff}} = 4801$ K, $\log g = 4.633$, and $[\text{Fe}/\text{H}] = -0.14$ dex) using the stellar parameters and abundances determined by Allende-Prieto et al. (2004). We only use as abundance indicators those features which were well reproduced in the template star. The chemical analysis is summarized in Table 2. The errors in the element abundances show their sensitivity to the uncertainties in the effective temperature (ΔT_{eff}), gravity ($\Delta \log g$), veiling (Δ_{veiling}), and the dispersion of the measurements from different spectral features (Δ_{σ}). In Table 2 we also state the number of features analyzed for each element.

The abundances of Ti and Si were mainly derived from several lines in the spectral region 5920–5960 Å where some telluric lines are present. However, since 74 spectra with

different radial velocities in the range ± 710 km s $^{-1}$ were combined to generate the average spectrum of the secondary star, these telluric lines must have been smoothed out.

The Mg abundance was derived from one spectral line (see Fig. 5) and the error associated with the dispersion of the measurements, σ , was assumed to be the average dispersion of Fe, Ca, and Ni abundances, and in this case, $\Delta_{\sigma} = \sigma$. The same prescription was adopted for the analysis of Al and Li (see Fig. 1 of Paper I). The best fit to the Li I 6708 Å feature provides an LTE abundance of $\log \epsilon(\text{Li})_{\text{LTE}} = 1.61 \pm 0.25$. We estimated the non-LTE abundance correction¹ for this element from the theoretical LTE and non-LTE curves of growth in Pavlenko & Magazzù

¹ $\Delta_{\text{NLTE}} = \log \epsilon(\text{X})_{\text{NLTE}} - \log \epsilon(\text{X})_{\text{LTE}}$.

TABLE 3
ELEMENT ABUNDANCE RATIOS IN XTE J1118+480

| Element | $[X/Fe]_{\text{XTE1118}}$ | $\Delta_{[X/Fe],\text{XTE1118}}^*$ | $[X/Fe]_{\text{stars}}$ | σ_{stars} | $\Delta_{\sigma,\text{stars}}$ |
|---------|---------------------------|------------------------------------|-------------------------|-------------------------|--------------------------------|
| Mg | 0.17 | 0.22 | 0.02 | 0.08 | 0.02 |
| Al | 0.42 | 0.15 | 0.14 | 0.10 | 0.02 |
| Si | 0.19 | 0.17 | -0.03 | 0.04 | 0.01 |
| Ca | -0.03 | 0.23 | -0.13 | 0.05 | 0.01 |
| Ti | 0.14 | 0.22 | 0.05 | 0.08 | 0.01 |
| Ni | 0.12 | 0.12 | -0.02 | 0.05 | 0.01 |

*Uncertainties in the element abundance ratios ($[X/Fe]$) in the secondary star in XTE J1118+480.

NOTE.— $[X/Fe]_{\text{stars}}$ indicate the average values of 24 stars with iron content in the range 0.01 to 0.35 corresponding to 1σ in the $[Fe/H]$ abundance of the secondary star in XTE J1118+480, taken from Gilli et al. (2006). The uncertainty in the average value of abundance ratios in the comparison sample is obtained as $\Delta_{\sigma,\text{stars}} = \sigma_{\text{stars}}/\sqrt{N}$, where σ_{stars} is the standard deviation of the measurements and N is the number of stars.

TABLE 4
SUPERNOVA/HYPERNOVA MODEL PARAMETERS

| M_{MS} | M_{He} | E_{51} | Z | $M(Fe)$ | M_{cut} | M_{fall} | $M_{\text{BH},i}^a$ | Abundance Pattern |
|-----------------|-----------------|----------|-------|------------|------------------|-------------------|---------------------|-------------------|
| 40 | 15.8 | 1 | 0.001 | 5.8982E-01 | 2.51 | 5.56 | 8.07 | Fig. 9a |
| 40 | 15.8 | 1 | 0.001 | 2.6581E-01 | 3.01 | 5.06 | 8.07 | Fig. 9a |
| 40 | 15.8 | 30 | 0.001 | 7.6394E-01 | 4.05 | 4.02 | 8.07 | Fig. 9b |
| 40 | 15.8 | 30 | 0.001 | 9.2867E-02 | 5.03 | 3.04 | 8.07 | Fig. 9b |
| 40 | 15.8 | 1 | 0.004 | 3.7283E-01 | 2.50 | 5.57 | 8.07 | Fig. 10a |
| 40 | 15.8 | 1 | 0.004 | 2.6649E-02 | 3.03 | 5.04 | 8.07 | Fig. 10a |
| 40 | 15.8 | 30 | 0.004 | 9.8590E-01 | 3.03 | 5.04 | 8.07 | Fig. 10b |
| 40 | 15.8 | 30 | 0.004 | 2.0354E-01 | 4.02 | 4.05 | 8.07 | Fig. 10b |
| 30 | 11 | 1 | 0.004 | 1.4667E-01 | 2.52 | 5.49 | 8.01 | Fig. 11a |
| 30 | 11 | 1 | 0.004 | 1.7806E-03 | 3.04 | 4.97 | 8.01 | Fig. 11a |
| 30 | 11 | 20 | 0.004 | 5.7203E-01 | 3.04 | 4.97 | 8.01 | Fig. 11b |
| 30 | 11 | 20 | 0.004 | 3.0448E-02 | 4.15 | 3.86 | 8.01 | Fig. 11b |
| 40 | 15.1 | 1 | 0.02 | 7.3775E-01 | 1.46 | 6.63 | 8.09 | Fig. 12a |
| 40 | 15.1 | 1 | 0.02 | 3.1602E-03 | 8.09 | 0 | 8.09 | Fig. 12a |
| 40 | 15.1 | 30 | 0.02 | 8.4572E-01 | 1.74 | 6.35 | 8.09 | Fig. 12b |
| 40 | 15.1 | 30 | 0.02 | 2.8515E-03 | 8.09 | 0 | 8.09 | Fig. 12b |
| 40 | 16 | 10 | 0.02 | 1.4337E-02 | 2.41 | 5.15 | 7.56 | Fig. 13a |
| 40 | 16 | 10 | 0.02 | 0 | 7.56 | 0 | 7.56 | Fig. 13a |
| 40 | 16 | 10 | 0.02 | 5.1974E-01 | 2.41 | 5.15 | 7.56 | Fig. 13b |
| 40 | 16 | 10 | 0.02 | 1.2716E-01 | 7.56 | 0 | 7.56 | Fig. 13b |

^a $M_{\text{BH},i}$ is the mass of the remnant after the explosion and before the secondary started to transfer matter onto the compact object. $M_{\text{BH},f} = 8.53 \pm 0.60 M_{\odot}$ is the observed mass of the black hole.

NOTE.—Supernova and hypernova explosion models used in Figs. 9-13. The quantities shown are the main-sequence mass, the mass of the He core, the explosion energy, $E_{51} = E_K/10^{51}$ erg, the ejected Fe mass, the metallicity of the model, the mass-cut, the mass of the fallback matter, and the final remnant mass. The mass are in units of M_{\odot} .

(1996). We found $\Delta_{\text{NLTE}} = 0.17$. Due to the weakness of the absorption we consider this abundance estimate given in Table 2 as an upper limit.

5. Discussion

As already discussed in Paper I, the Fe abundance of the secondary star is slightly higher than solar, but similar to that of many stars in the solar neighborhood. The abundances of other elements listed in Table 2 relative to iron are compared in Fig. 7 with the Galactic trends of these elements in the relevant range of metallicities. Moderate anomalies are found only for Al. In Table 3 we show the element abundance ratios in the secondary star in XTE J1118+480 and the average values in stars with iron content in the range $0.01 < [\text{Fe}/\text{H}] < 0.35$, the comparison sample, corresponding to a 1σ uncertainty in the iron abundance of the companion star. Whereas Ca and Ti are consistent with the average values of the comparison sample, Ni and Si, at 1σ , and especially Al, at 2σ , appear to be more abundant than the average values of the stars in the comparison sample.

The present location and space-velocity components (U , V) of the system might suggest that the system belongs to the Galactic halo, but the derived metallicity makes this possibility less likely. One could include the metallicity in the expression given in Bensby et al. (2005) to estimate the relative likelihoods that a star belongs to the Galactic thin disk, thick disk, and halo. The equations could be written as follows:

$$\begin{aligned} P_{\text{thin-disk}} &= f_{\text{D}} \frac{P_{\text{D}}}{P}, \\ P_{\text{thick-disk}} &= f_{\text{TD}} \frac{P_{\text{TD}}}{P}, \\ P_{\text{halo}} &= f_{\text{H}} \frac{P_{\text{H}}}{P}, \end{aligned}$$

$$\begin{aligned} P_i &= K_i \times \exp \left[-\frac{U^2_{\text{LSR}}}{2\sigma^2_{U_i}} - \frac{(V_{\text{LSR}} - V_{\text{asym},i})^2}{2\sigma^2_{V_i}} \right] \\ &\times \exp \left[-\frac{W^2_{\text{LSR}}}{2\sigma^2_{W_i}} - \frac{([\text{Fe}/\text{H}] - [\text{Fe}/\text{H}]_{\text{asym},i})^2}{2\sigma^2_{[\text{Fe}/\text{H}]_i}} \right], \\ P &= f_{\text{D}} P_{\text{D}} + f_{\text{TD}} P_{\text{TD}} + f_{\text{H}} P_{\text{H}}, \\ \text{and } K_i &= \frac{1}{(2\pi)^3 \sigma_{U_i} \sigma_{V_i} \sigma_{W_i} \sigma_{[\text{Fe}/\text{H}]_i}}, \end{aligned}$$

where the subscript i indicates the three populations D (thin disk), TD (thick disk), and H (halo). The total probability, P , takes into account the fraction of stars belonging to each population in the solar neighborhood ($f_{\text{D}} = 0.94$, $f_{\text{TD}} = 0.06$, and $f_{\text{H}} = 0.0015$; Bensby et al. 2003). The velocity distributions of each population with respect to the local standard of rest (LSR) are centered at zero except for the component V_{LSR} , whose center is displaced according to $V_{\text{asym},i}$ (with $V_{\text{asym},D} = -15 \text{ km s}^{-1}$, $V_{\text{asym},TD} = -46 \text{ km s}^{-1}$, and $V_{\text{asym},H} = -220 \text{ km s}^{-1}$). The metallicity distributions have been characterized with $[\text{Fe}/\text{H}]_{\text{asym},D} = -0.1$, $[\text{Fe}/\text{H}]_{\text{asym},TD} = -0.7$, and $[\text{Fe}/\text{H}]_{\text{asym},H} = -1.4$, as well as with $\sigma_{[\text{Fe}/\text{H}]_D} = 0.2$, $\sigma_{[\text{Fe}/\text{H}]_{TD}} = 0.24$, and $\sigma_{[\text{Fe}/\text{H}]_H} = 0.5$, according to Allende Prieto et al. (2004, 2006). Thus, the probability that a star with the Galactic space velocity components of this system (Mirabel et al. 2001; $U = -105 \pm 16 \text{ km s}^{-1}$, $V = -98 \pm 16 \text{ km s}^{-1}$, $W = -21 \pm 10 \text{ km s}^{-1}$) and metallicity $[\text{Fe}/\text{H}] = 0.18$ belongs to the Galactic halo is less than 0.1%. Moreover, the kinematics alone suggest thick-disk rather than halo membership, although the high metallicity of the secondary star favors thin-disk membership. However, the system could also have originated in a satellite galaxy. In particular, its galactocentric orbit (Mirabel et al. 2001) is marginally consistent with the equatorial orbit of the stream of the dwarf galaxy in Canis Major, although its present Galactic latitude differs by more than 40° from the $l-b$ distribution of the remnant of this dwarf galaxy, accreted by the Milky Way (Martin et

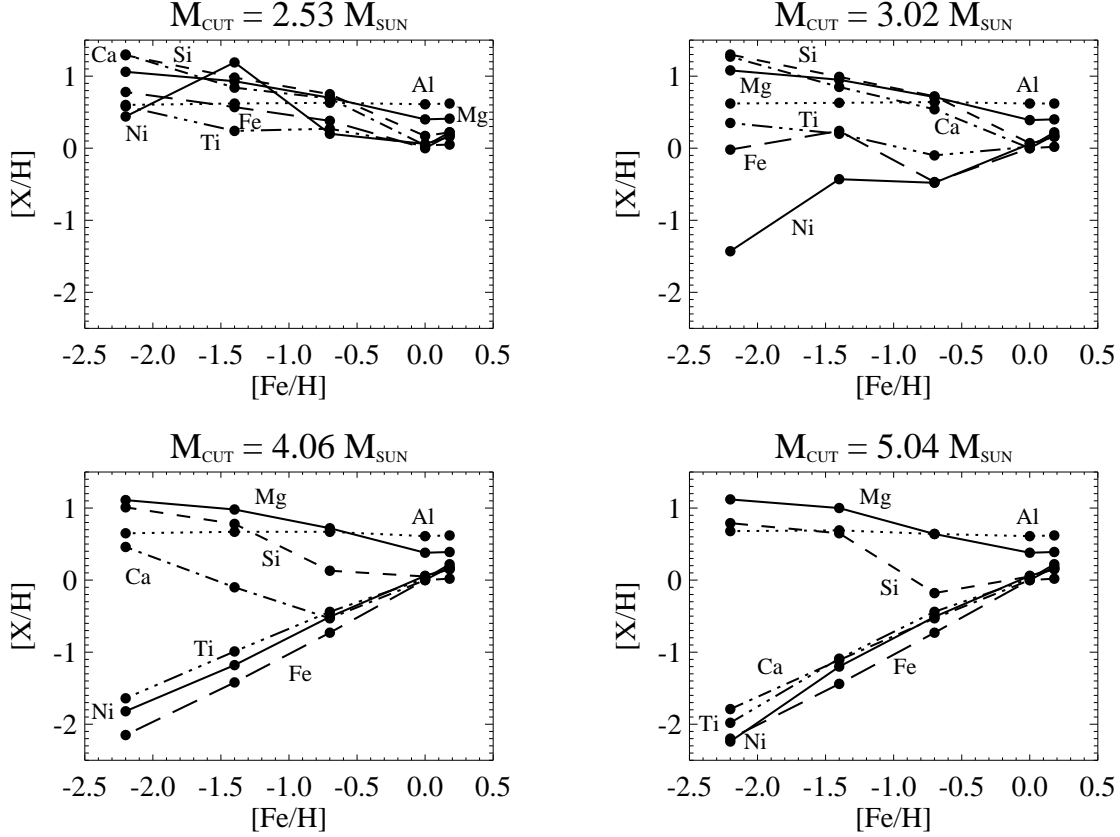


Fig. 8.— Chemical composition of the secondary atmosphere contaminated with nucleosynthetic products of a $40 M_{\odot}$ spherically symmetric core-collapse SN explosion model ($M_{\text{He}} \approx 15\text{--}16 M_{\odot}$) for different metallicities and mass-cuts, M_{cut} .

al. 2004).

The system could also have originated as a consequence of an encounter of an ancient black hole of the Galactic halo with a single star or a binary of two solar-type stars of the Galactic disk. However, this possibility is very unlikely due to the extremely low density of stars in the disk (~ 0.006 stars/pc³; Mihalas & Binney 1981). The orbit of the system integrated backward in time never crossed the Galactic plane through the inner 2 kpc (Gualandris et al. 2005), so high-density regions near the Galactic center are discarded. Portegies Zwart et al. (1997b) have modeled the encounter of black holes in high-density systems. In high-density systems, where the den-

sity of stars is $\sim 4 \times 10^6$ stars/pc³ (10^9 times higher than in the Galactic disk), a black hole spends 1.5 Gyr before it suffers a tidal capture by a main-sequence star. In addition, the cases where a black hole can capture an isolated star or one star of a binary require very stringent constraints on the closest approach and impact velocity (Benz & Hills 1992; Hills 1991). All these reasons make this possibility very unlikely.

Therefore, in conclusion, the present location, velocity, and metallicity of the secondary star in XTE J1118+48 suggest that the black hole formed in a supernova/hypernova explosion that occurred within the binary system. This explosive event must have either pro-

vided a kick to the system if it was formed in the thin disk, or enriched significantly the atmosphere of the secondary star if the system formed in the thick disk or halo.

The present orbital separation between the compact object and the secondary star has been estimated to be $a_c \approx 2.67 R_\odot$ (Gelino et al. 2006). Thus, the secondary star could have captured a significant amount of the ejected matter in the SN explosion that formed the compact object. The chemical composition of the secondary star may provide information on the chemical composition of the progenitor of the compact object, and therefore on the formation region (thin disk, thick disk, or halo) of the binary system. We will now discuss the possibility that the SN explosion of the massive progenitor enriched the secondary star from different initial metallicities.

5.1. Spherical Explosion

Gelino et al. (2006) derived a current black hole mass of $M_{\text{BH},f} = 8.53 \pm 0.60 M_\odot$ and secondary mass of $M_{2,f} = 0.37 \pm 0.03 M_\odot$. Using near-UV spectroscopic observations of the accretion disk, Haswell et al. (2002) suggested that the material accreted onto the compact object is substantially CNO processed, indicating that the initial mass of the secondary star could have been as high as $\sim 1.5 M_\odot$. Hereafter we will adopt an initial secondary mass of $M_{2,i} = 1 M_\odot$ and a black hole mass of $M_{\text{BH},i} = 8 M_\odot$.

A binary system such as XTE J1118+480 will survive a spherical SN explosion if the ejected mass $\Delta M = M_{\text{He}} - M_{\text{BH},i} \leq (M_{\text{He}} + M_{2,i})/2$ (Hills 1983). This implies a mass of the He core before the SN explosion of $M_{\text{He}} \leq 17 M_\odot$. Using the expressions given by Portegies Zwart et al. (1997a, and references therein), we inferred a He core radius of $R_{\text{He}} \approx 2 - 3 R_\odot$ for He core masses in the range $M_{\text{He}} \approx 8.5 - 17 M_\odot$. We will as-

sume that the post-SN orbital separation after tidal circularization of the orbit is in the range $a_{c,i} \approx 4 - 6 R_\odot$, since the secondary must have experienced mass and angular momentum losses during the binary evolution until reaching its present configuration, with $a_{c,f} \approx 2.67 R_\odot$.

Assuming a pre-SN circular orbit and an instantaneous spherically symmetric ejection (that is, shorter than the orbital period), one can estimate the pre-SN orbital separation, a_0 , using the relations given by van den Heuvel & Habets (1984): $a_0 = a_{c,i} \mu_f$, where $\mu_f = (M_{\text{BH},i} + M_{2,i})/(M_{\text{He}} + M_{2,i})$. We find $a_0 \approx 3-5$, essentially depending on the adopted values of M_{He} and $a_{c,i}$. At the time of the SN explosion ($\sim 5-6$ Myr; Brunish & Truran 1982), a $1 M_\odot$ secondary star, still in its pre-main-sequence evolution, has a radius $R_{2,i} \approx 1.3 R_\odot$ and a convective zone of mass $M_{\text{cz}} \approx 0.652 M_\odot$ (D’Antona & Mazzitelli 1994). Thus, the amount of mass deposited on the secondary can be estimated as $m_{\text{cap}} = \Delta M (\pi R_{2,i}^2 / 4\pi a_0^2) f_{\text{cap}} M_\odot$, where f_{cap} is the fraction of mass, ejected within the solid angle subtended by the secondary star, that is eventually captured. We assume that the captured mass, m_{cap} , is efficiently mixed with the mass of the convective zone, M_{cz} .

We compute the expected abundances in the atmosphere of the secondary star after the pollution from the progenitor of the compact object as in González Hernández et al. (2004). We used $40 M_\odot$ spherically symmetric core-collapse explosion models ($M_{\text{He}} \approx 15.1-16.1 M_\odot$) for different metallicities ($Z = 0, 0.001, 0.004, 0.02$) and explosion energies (Umeda & Nomoto, 2002, 2005; Tominaga, Umeda & Nomoto 2007). These models imply $\Delta M \approx 7-8 M_\odot$ and need small capture efficiencies of $f_{\text{cap}} \lesssim 0.1$ (i.e., 10%) to increase significantly the metal content of the secondary star. On the other hand, the use of $30 M_\odot$ models ($M_{\text{He}} \approx 8.5-11.2 M_\odot$) would

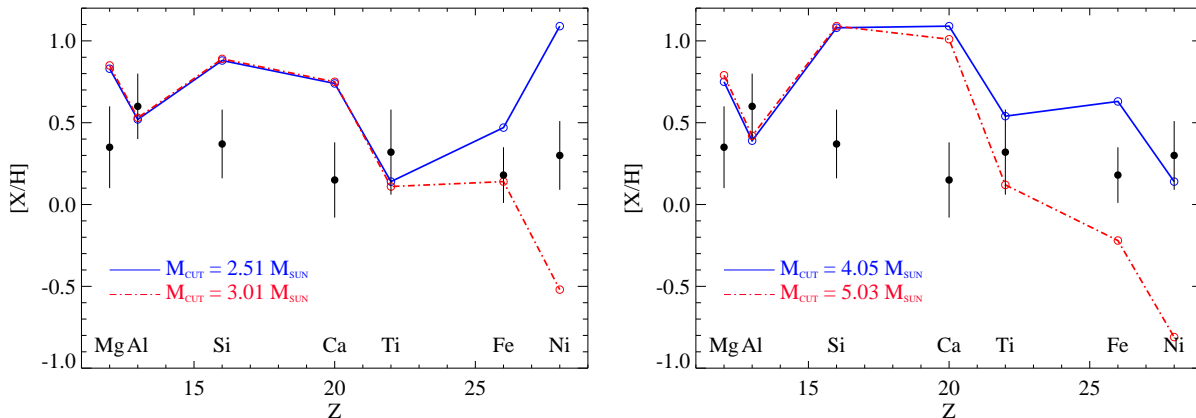


Fig. 9.— Left panel: Observed abundances (filled circles with error bars) in comparison with the expected abundances in the secondary star after having captured 17.5% of the matter ejected within the solid angle subtended by the secondary from a metal-poor ($Z = 0.001$) $40 M_{\odot}$ spherically symmetric supernova explosion ($M_{\text{He}} = 15.8 M_{\odot}$) with $E_K = 10^{51}$ erg for two different mass-cuts, $M_{\text{cut}} = 2.51 M_{\odot}$ (solid line with open circles) and $M_{\text{cut}} = 3.01 M_{\odot}$ (dashed-dotted line with open circles). The initial abundances of the secondary star were adopted for the average abundances of halo stars with $[\text{Fe}/\text{H}] = -1.4 \pm 0.2$, and the initial orbital distance was $a_{c,i} \approx 6 R_{\odot}$. Right panel: same as left panel but for a spherically symmetric hypernova explosion ($E_K = 30 \times 10^{51}$ erg) for two different mass-cuts, $M_{\text{cut}} = 4.05 M_{\odot}$ (solid line with open circles) and $M_{\text{cut}} = 5.03 M_{\odot}$ (dashed-dotted line with open circles).

require $f_{\text{cap}} \approx 0.9$ –1. These models would also provide a different mass fraction of each element at each value of the mass-cut (the mass that initially collapsed forming the compact remnant). For more details in the models, see Tominaga, Umeda & Nomoto (2007).

The explosion energy, $E_K = 1 \times 10^{51}$ erg and $E_K = (20 - 30) \times 10^{51}$ erg for the supernova (SN) and hypernova (HN) models (respectively), is deposited instantaneously in the central region of the progenitor core to generate a strong shock wave. The subsequent propagation of the shock wave is followed through a hydrodynamic code (Umeda & Nomoto 2002, and references therein). In our simple model, we have assumed different mass-cuts, fallback masses, and a mixing factor of 1 which assumes that all fallback matter is well mixed with the ejecta. The amount of fallback, M_{fall} , is the difference between the final remnant mass, $M_{\text{BH},i}$, and the initial remnant mass of the explosion, M_{cut} . We should recall here the ejected mass, ΔM , which is

equal to $M_{\text{He}} - M_{\text{BH},i}$, where M_{He} is the mass of the He core.

We use SN/HN models to provide us with the yields of the explosion before radiative decay of element species. We then compute the integrated, decayed yields of the ejecta by adopting a mass-cut and by mixing all the material above the mass-cut. Finally, we calculate the composition of the matter captured by the secondary star, and we mix it with the material of its convective envelope.

In Fig. 8 we show the expected abundances of the secondary star after contamination from the nucleosynthetic products of the SN explosion ($E_K = 1 \times 10^{51}$ erg) of $M_{\text{He}} \approx 15$ –16 M_{\odot} progenitor stars. The initial abundances of the secondary star have been estimated from the average abundances of halo stars with a metallicity of $[\text{Fe}/\text{H}] \approx -2.2$ (from Cayrel et al. 2004) and $[\text{Fe}/\text{H}] \approx -1.4$ (from Jonsell et al. 2005), thick-disk stars with $[\text{Fe}/\text{H}] \approx -0.7$ (from Jonsell et al. 2005), and thin-disk stars with $[\text{Fe}/\text{H}] \approx 0$

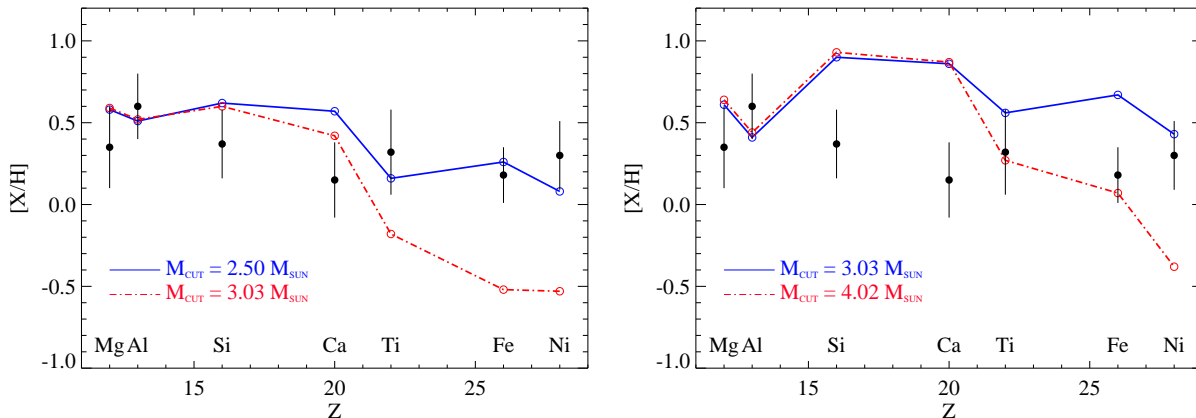


Fig. 10.— Left panel: Observed abundances (filled circles with error bars) in comparison with the expected abundances in the secondary star after having captured the 15.5% of the matter ejected within the solid angle subtended by the secondary from a metal-poor ($Z = 0.004$) $40 M_{\odot}$ spherically symmetric supernova explosion ($M_{\text{He}} = 15.8 M_{\odot}$) with $E_K = 10^{51}$ erg for two different mass-cuts, $M_{\text{cut}} = 2.50 M_{\odot}$ (solid line with open circles) and $M_{\text{cut}} = 3.03 M_{\odot}$ (dashed-dotted line with open circles). The initial abundances of the secondary star were adopted for the average abundances of thick-disk stars with $[\text{Fe}/\text{H}] = -0.7 \pm 0.2$, and the initial orbital distance was $a_{c,i} \approx 6 R_{\odot}$. Right panel: same as left panel but for a spherically symmetric hypernova explosion ($E_K = 30 \times 10^{51}$ erg) for two different mass-cuts, $M_{\text{cut}} = 3.03 M_{\odot}$ (solid line with open circles) and $M_{\text{cut}} = 4.02 M_{\odot}$ (dashed-dotted line with open circles).

and $[\text{Fe}/\text{H}] \approx 0.18$ (from Gilli et al. 2006). For each simulation at each metallicity, we have fixed the f_{cap} factor at a value that allows us to approximately match the observed aluminum abundance.

We should remark that for a given model at a given metallicity, once the capture efficiency is fixed, the aluminum (Al) abundance in the secondary star hardly depends on the mass-cut. Thus, the fact that the Al abundance in Fig. 8 is almost constant with metallicity is because we have adopted different f_{cap} factors for different metallicities. These f_{cap} factors are higher for lower metallicities since greater amounts of captured material are needed to achieve the observed Al abundance in the secondary star. For other figures in this paper, the f_{cap} factor was changed until an abundance of $[\text{Al}/\text{H}] \approx 0.5$ dex was obtained, compatible with the observed abundance within the uncertainties.

From Fig. 8 one can see that while Mg and

Al remain significantly enhanced (above solar abundances) for all mass-cuts at all metallicities, Si, Ca, Ti, Fe, and Ni are quite sensitive to the mass-cut of the model. Thus, for metallicities below -1.4 dex, only $M_{\text{cut}} \lesssim 3 M_{\odot}$ is able to enhance sufficiently the Ti, Fe, and Ni, whereas Ca and Si remain quite overabundant for $M_{\text{cut}} \lesssim 4 M_{\odot}$ and $5 M_{\odot}$ (respectively) at all metallicities. We should note that for metallicities $[\text{Fe}/\text{H}] \lesssim -1.4$ dex (i.e., $Z \lesssim 0.001$), the expected abundances in the secondary star do not depend on the initial abundances but on the SN yields. Thus, we found different expected abundances of the secondary between $[\text{Fe}/\text{H}] \approx -1.4$ dex and $[\text{Fe}/\text{H}] \approx -2.2$ dex because we used the SN $Z = 0.001$ model and the SN $Z = 0$ model, respectively.

5.2. Formation in the Halo

The kinematics of the system, at least U and V , resemble those of halo stars, and there-

TABLE 5
METAL-POOR SUPERNOVA/HYPERNOVA EXPLOSION MODELS IN XTE J1118+480

| ELEMENT | [X/H] OBSERVED ^a | [X/H] ₀ ^b | [X/H] EXPECTED ^d | | | |
|--|-----------------------------|---------------------------------|---------------------------------|---------------------|----------------------|---------------------|
| | | | Supernova | | Hypernova | |
| | | | $M_{\text{cut,low}}^{\text{c}}$ | $M_{\text{cut,up}}$ | $M_{\text{cut,low}}$ | $M_{\text{cut,up}}$ |
| 40 M _⊙ explosion model of $Z = 0.001$ | | | | | | |
| Mg | 0.35 | -1.08 | 0.83 | 0.85 | 0.75 | 0.79 |
| Al | 0.60 | -1.27 | 0.52 | 0.53 | 0.39 | 0.42 |
| Si | 0.37 | -1.13 | 0.88 | 0.89 | 1.08 | 1.09 |
| Ca | 0.15 | -1.12 | 0.74 | 0.75 | 1.09 | 1.01 |
| Ti | 0.32 | -1.15 | 0.14 | 0.11 | 0.54 | 0.12 |
| Fe | 0.18 | -1.46 | 0.47 | 0.14 | 0.63 | -0.22 |
| Ni | 0.30 | -1.48 | 1.09 | -0.52 | 0.14 | -0.81 |
| O | ... | -0.76 | 0.75 | 0.77 | 0.69 | 0.73 |
| C | ... | -0.86 | -0.54 | -0.53 | -0.60 | -0.58 |
| 40 M _⊙ explosion model with $Z = 0.004$ | | | | | | |
| Mg | 0.35 | -0.41 | 0.58 | 0.59 | 0.61 | 0.64 |
| Al | 0.60 | -0.46 | 0.51 | 0.52 | 0.41 | 0.44 |
| Si | 0.37 | -0.50 | 0.62 | 0.60 | 0.90 | 0.93 |
| Ca | 0.15 | -0.54 | 0.57 | 0.42 | 0.86 | 0.87 |
| Ti | 0.32 | -0.50 | 0.16 | -0.18 | 0.56 | 0.27 |
| Fe | 0.18 | -0.75 | 0.26 | -0.52 | 0.67 | 0.07 |
| Ni | 0.30 | -0.73 | 0.08 | -0.53 | 0.43 | -0.38 |
| O | ... | -0.26 | 0.71 | 0.73 | 0.67 | 0.69 |
| C | ... | -0.35 | 0.10 | 0.11 | 0.06 | 0.08 |
| 30 M _⊙ explosion model with $Z = 0.004$ | | | | | | |
| Mg | 0.35 | -0.41 | 0.60 | 0.62 | 0.57 | 0.62 |
| Al | 0.60 | -0.46 | 0.52 | 0.54 | 0.40 | 0.45 |
| Si | 0.37 | -0.50 | 0.77 | 0.54 | 1.02 | 0.95 |
| Ca | 0.15 | -0.54 | 0.72 | 0.17 | 1.03 | 0.82 |
| Ti | 0.32 | -0.50 | 0.18 | -0.41 | 0.66 | 0.01 |
| Fe | 0.18 | -0.75 | 0.14 | -0.71 | 0.71 | -0.32 |
| Ni | 0.30 | -0.73 | -0.43 | -0.54 | 0.40 | -0.40 |
| O | ... | -0.26 | 0.75 | 0.78 | 0.69 | 0.74 |
| C | ... | -0.35 | 0.02 | 0.03 | -0.04 | -0.01 |

^aObserved abundances of the secondary star in XTE J1118+480.

^bInitial abundances assumed for the secondary star in XTE J1118+480, see text. The initial C and O abundances of the thick-disk model ($[X/H]_0 = -0.7$) were adopted from Ecuivillon et al. (2004, 2006).

^c $M_{\text{cut,low}}$ and $M_{\text{cut,up}}$ are the lower and upper mass-cut adopted in the model computation. See the exact value in the captions of Figs. 9-11.

^dExpected abundances of the secondary star.

NOTE.—Expected abundances in the secondary atmosphere contaminated with nucleosynthetic products of metal-poor explosion models for two different explosion energies and mass-cuts, presented in Figs. 9-11.

fore a significant kick during the black hole formation process appears unnecessary. Thus, a spherically symmetric SN explosion would provide the desired kick velocity to match the current velocity components of the system from initial velocities similar to those of halo stars. However, due to the extremely low metallicities of halo stars, it is required that the secondary captured enough matter from the ejecta to reach the current abundances.

In Fig. 9 we compare the observed abundances with the expected abundances in the secondary star for two different explosion energies and mass-cuts using a metal-poor $40 M_{\odot}$ progenitor model. In these simulations, the mass-cut is sampled according to the mass bins given in the explosion models, from $\sim 1.5 M_{\odot}$ to $8 M_{\odot}$ in steps of ~ 0.5 and $1 M_{\odot}$. The adopted mass-cuts shown in Fig. 9 were selected from those which provided better fits to the observed abundances. The initial abundances of the secondary have been estimated from the average abundances of halo stars with $[\text{Fe}/\text{H}] \approx -1.4$ from Jonsell et al. (2005). The value of f_{cap} has been adjusted until the observed aluminum abundance was roughly reproduced, providing $f_{\text{cap}} \approx 0.17$. The parameters of the explosion models used in Fig. 9 – 13 are given in Table 4. In Table 5 we show the expected abundances of the secondary star after contamination from metal-poor SN/HN explosion models.

With a supernova model, shown in the left panel of Fig. 9, it is not possible to recover the observed abundances because these models produce too much Mg and Ca regardless of the Fe abundance obtained; in addition, the Ni abundance is strongly dependent on the mass-cut. The hypernova model, displayed in the right panel, makes it even more difficult to fit the observed abundances since this model creates too much Ca relative to Fe and Ni. As inferred from Fig. 8, a model with initial abundances at $[\text{Fe}/\text{H}] \approx -2.2$ (Cayrel et al.

2004) would also not be successful in reproducing the observed abundances due to the tremendous and different sensitivity of each element to the mass-cut.

In conclusion, neither of these very metal-poor models is able to reproduce the observed abundances. We also try to fit the observed abundances using a metal-poor $30 M_{\odot}$ explosion model, but the agreement is even worse than for $40 M_{\odot}$ models, again due to the strong sensitivity of the each element abundance to the mass-cut. The comparison of the observed abundances with SN yields allows us to rule out a Galactic halo origin for this black hole binary.

5.3. Formation in the Thick Disk

The space-velocity components of the system are comparable to those of thick-disk stars, and its present location 1.6 kpc above the Galactic plane is slightly higher than the scale height of thick-disk stars (~ 0.8 – 1.3 kpc; Reylé & Robin 2001; Chen 1997); thus, a strong kick during the SN explosion would not be required. A spherically symmetric SN explosion of a $15.8 M_{\odot}$ and $11 M_{\odot}$ He core provides an impulse of ~ 60 and $\sim 20 \text{ km s}^{-1}$, respectively. However, an enrichment from the typical abundances of thick-disk stars would have been necessary. In the simulations, the initial abundances were assumed to be the average values of thick-disk stars with $[\text{Fe}/\text{H}] \approx -0.7$ from Jonsell et al. (2005).

In Fig. 10 we compare the expected abundances from a $40 M_{\odot}$ explosion model for two energies and mass-cuts (see also Table 5). The left panel shows the expected abundances from a SN model which seems to better approach the observed abundances than those of halo-like metallicities. As in the previous figure, the f_{cap} factor was changed until an abundance of $[\text{Al}/\text{H}] \approx 0.5$ dex was obtained, compatible with the observed abundance within the uncertainties. For the mass-

TABLE 6
METAL-RICH SUPERNOVA/HYPERNOVA EXPLOSION MODELS IN XTE J1118+480

| | | [X/H] EXPECTED ^d | | | | |
|--|-----------------------------|---------------------------------|---|------------------------------|----------------------|---------------------|
| ELEMENT | [X/H] OBSERVED ^a | [X/H] ₀ ^b | $M_{\text{cut,low}}$ ^c | $M_{\text{cut,up}}$ | $M_{\text{cut,low}}$ | $M_{\text{cut,up}}$ |
| Spherical explosion model of $Z = 0.02$ | | | | | | |
| | | | Supernova | Hypernova | | |
| Mg | 0.35 | 0.17 | 0.32 | 0.30 | 0.32 | 0.30 |
| Al | 0.60 | 0.29 | 0.50 | 0.50 | 0.48 | 0.50 |
| Si | 0.37 | 0.12 | 0.22 | 0.14 | 0.28 | 0.14 |
| Ca | 0.15 | 0.02 | 0.09 | 0.02 | 0.15 | 0.02 |
| Ti | 0.32 | 0.20 | 0.24 | 0.21 | 0.34 | 0.21 |
| Fe | 0.18 | 0.18 | 0.30 | 0.18 | 0.32 | 0.18 |
| Ni | 0.30 | 0.13 | 0.35 | 0.15 | 0.32 | 0.15 |
| O | ... | 0.18 | 0.33 | 0.33 | 0.33 | 0.33 |
| C | ... | 0.11 | 0.16 | 0.16 | 0.15 | 0.16 |
| Aspherical explosion model with $Z = 0.02$ | | | | | | |
| | | | Angle ^e = $0^\circ - 15^\circ$ | Angle = $0^\circ - 90^\circ$ | | |
| Mg | 0.35 | 0.17 | 0.34 | 0.32 | 0.34 | 0.35 |
| Al | 0.60 | 0.29 | 0.51 | 0.48 | 0.50 | 0.51 |
| Si | 0.37 | 0.12 | 0.24 | 0.18 | 0.35 | 0.26 |
| Ca | 0.15 | 0.02 | 0.05 | 0.02 | 0.22 | 0.11 |
| Ti | 0.32 | 0.20 | 0.21 | 0.20 | 0.41 | 0.35 |
| Fe | 0.18 | 0.18 | 0.18 | 0.18 | 0.28 | 0.22 |
| Ni | 0.30 | 0.13 | 0.13 | 0.13 | 0.34 | 0.23 |
| O | ... | 0.18 | 0.37 | 0.35 | 0.38 | 0.39 |
| C | ... | 0.11 | 0.12 | 0.13 | 0.12 | 0.13 |

^aObserved abundances of the secondary star in XTE J1118+480.

^bInitial abundances assumed for the secondary star in XTE J1118+480, see text. The initial C and O abundances of the metal-rich models were adopted from Ecuivillon et al. (2004, 2006).

^c $M_{\text{cut,low}}$ and $M_{\text{cut,up}}$ are the lower and upper mass-cut adopted in the model computation. See the exact value in the captions of Figs. 12 and 13.

^dExpected abundances of the secondary star.

^eAngular range, measured from the equatorial plane, in which all the ejected material in the explosion has been completely mixed for each velocity point.

NOTE.—Expected abundances in the secondary atmosphere contaminated with nucleosynthetic products of metal-rich explosion models for two different mass-cuts and symmetries, presented in Figs. 12 and 13.

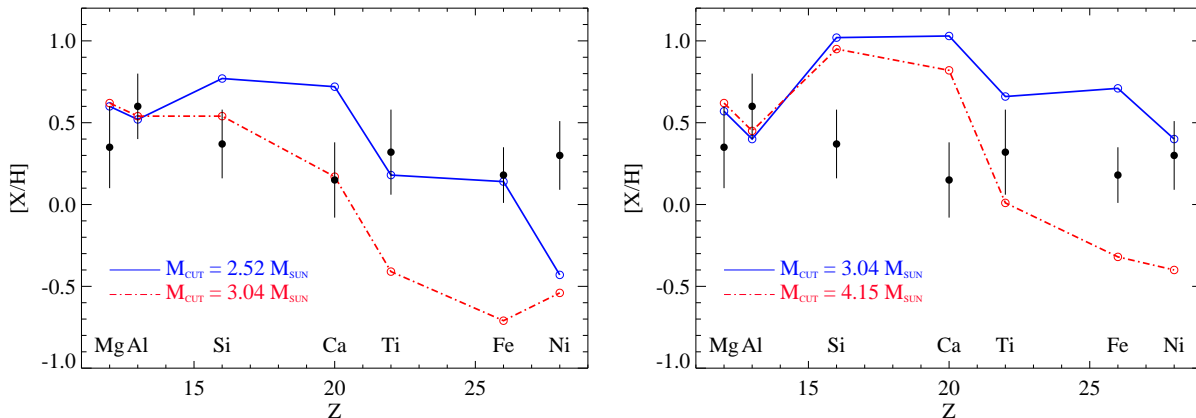


Fig. 11.— Left panel: Observed abundances (filled circles with error bars) in comparison with the expected abundances in the secondary star after having captured 90% of the matter ejected within the solid angle subtended by the secondary from a metal-poor ($Z = 0.004$) $30 M_{\odot}$ spherically symmetric supernova explosion ($M_{\text{He}} = 11 M_{\odot}$) with $E_K = 10^{51}$ erg for two different mass-cuts, $M_{\text{cut}} = 2.52 M_{\odot}$ (solid line with open circles) and $M_{\text{cut}} = 3.04 M_{\odot}$ (dashed-dotted line with open circles). The initial abundances of the secondary star were adopted for the average abundances of the thick-disk stars with $[\text{Fe}/\text{H}] = -0.7 \pm 0.2$, and the initial orbital distance was $a_{c,i} \approx 6 R_{\odot}$. Right panel: same as left panel but for a spherically symmetric hypernova explosion ($E_K = 20 \times 10^{51}$ erg) for two different mass-cuts, $M_{\text{cut}} = 3.04 M_{\odot}$ (solid line with open circles) and $M_{\text{cut}} = 4.15 M_{\odot}$ (dashed-dotted line with open circles).

cut of $2.50 M_{\odot}$, the model roughly fits the observed abundances except for Ca, which appears enhanced in the model by a factor of 2.6. Better agreement with Ca could be obtained if the f_{cap} factor is lowered, but then Al, Ni, and Ti would not match their observed abundances. If we increase the mass-cut up to $3.03 M_{\odot}$, the Ca abundance only decreases 0.15 dex whereas Ti, Fe, and Ni decrease by a factor of 2, 6, and 4 (respectively), which makes the model unable to fit the observed abundances. The hypernova case offers worse results since Si and Ca are no longer reproduced, and Fe and Ni cannot be fitted at the same time.

For this metallicity we have also explored the $30 M_{\odot}$ explosion model. The results are displayed in Fig. 11. In the left panel the SN model is compared with the observations. For the lower mass-cut, at $2.52 M_{\odot}$, the model provides too high Si and Ca abundances and too low Ni abundance, whereas for a mass-cut of $3.04 M_{\odot}$, the observed Ti, Fe, and Ni

abundances are too high in comparison with the model predictions. In the hypernova case (right panel of Fig. 11), at these low mass-cuts the model produces too large amounts of Si and Ca; in addition, Ti, Fe, and Ni are too sensitive to the location of the mass-cut.

Despite the fact that none of the explosion models explored is able to fairly reproduce the observed abundances in the secondary star, all of the models require vigorous mixing between the fallback matter and the final ejected matter (Kifonidis et al. 2000). For instance, in the $15.8 M_{\odot}$ He core model, all of the material above the mass-cut placed at $2.50 M_{\odot}$ should be well mixed in order to convey heavy elements like Fe and Ni to the outer layers of the explosion, which might make more unlikely a Galactic thick-disk origin for XTE J1118+480.

5.4. Formation in the Thin Disk

In this scenario, the system must have acquired an impulse during the formation of the

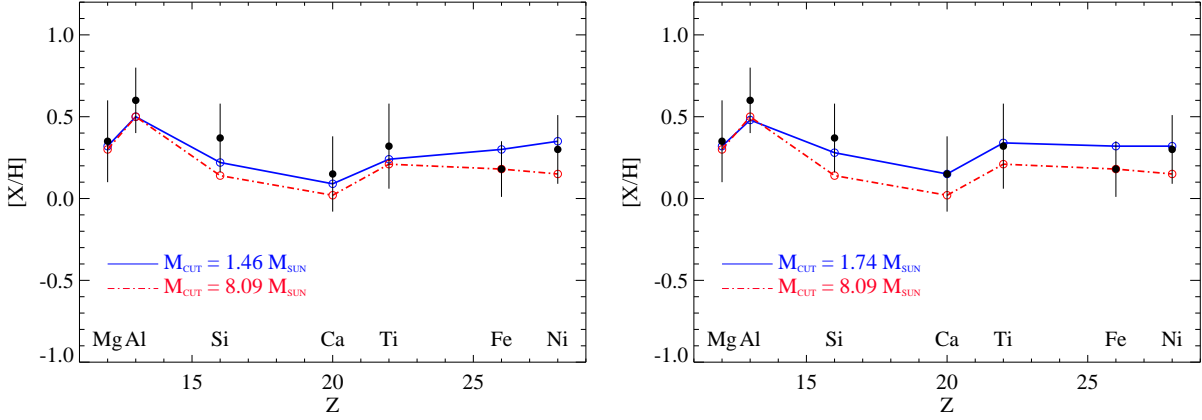


Fig. 12.— Left panel: Observed abundances (filled circles with error bars) in comparison with the expected abundances in the secondary star after having captured the 5% of the matter ejected within the solid angle subtended by the secondary from a metal-poor ($Z = 0.02$) $40 M_{\odot}$ spherically symmetric supernova explosion ($M_{\text{He}} = 15.1 M_{\odot}$) with $E_K = 10^{51}$ erg for two different mass-cuts, $M_{\text{cut}} = 1.46 M_{\odot}$ (solid line with open circles) and $M_{\text{cut}} = 8.09 M_{\odot}$ (dashed-dotted line with open circles). The initial abundances of the secondary star were adopted for the average abundances of thin-disk stars with $[\text{Fe}/\text{H}] = 0.0 \pm 0.2$. Right panel: same as left panel but for a spherically symmetric hypernova explosion ($E_K = 30 \times 10^{51}$ erg) for two different mass-cuts, $M_{\text{cut}} = 1.74 M_{\odot}$ (solid line with open circles) and $M_{\text{cut}} = 8.09 M_{\odot}$ (dashed-dotted line with open circles).

black hole that pushes it up from a Galactic plane orbit to the current halo orbit. The system should have been accelerated to a peculiar space velocity of $\sim 180 \text{ km s}^{-1}$ (Gualandris et al. 2005) to reach its present location, requiring an asymmetric kick. It has been suggested that such kicks can be imparted during the birth of nascent neutron stars, due to asymmetric mass ejection and/or an asymmetry in the neutrino emission (Lai et al. 2001, and references therein).

Podsiadlowski et al. (2002) proposed that the black hole in Nova Sco 1994 could have formed in a two-stage process where the initial collapse led to the formation of a neutron star accompanied by a substantial kick and the final mass of the compact remnant was achieved by matter that fell back after the initial collapse. However, the black hole mass in Nova Sco 1994 is estimated to be $\sim 5.4 M_{\odot}$ (Beer & Podsiadlowski 2002), while the black hole in XTE J1118+480 has a mass of $\sim 8 M_{\odot}$ which would require a fallback

mass of $\sim 6.6 M_{\odot}$ if we assume $\sim 1.4 M_{\odot}$ for a canonical neutron star. This scenario might take place in the context of collapsar models where the black hole would be formed in a mild explosion and substantial fallback (up to $\sim 5 M_{\odot}$ is expected) as proposed by MacFadyen et al. (2001). Asymmetric mass ejection would relax this requirement, providing enough impulse to the system to be launched into its present orbit from the Galactic plane.

In Fig. 12, we compare the expected abundances from the explosion of a $15.1 M_{\odot}$ He core with the observed abundances of the secondary star (see also Table 6). As in the previous figures, the f_{cap} factor was changed until an abundance of $[\text{Al}/\text{H}] \approx 0.5$ dex was obtained, compatible with the observed abundance within the uncertainties. The initial abundances were assumed to match the average values of disk stars with similar iron content, which are provided in Table 3. For both the SN model (left panel) and the hypernova model (right panel), the observed el-

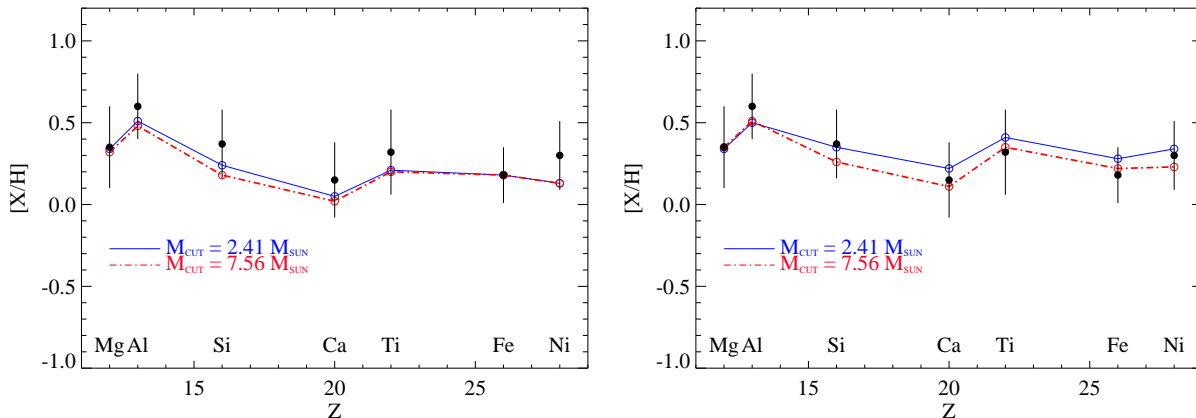


Fig. 13.— Left panel: Observed abundances (filled circles with error bars) in comparison with the expected abundances in the secondary star after having captured the 5% of the matter ejected within the solid angle subtended by the secondary from a non-spherically symmetric supernova explosion of $E_K = 10^{52}$ erg for two different mass-cuts, $M_{\text{cut}} = 2.41 M_{\odot}$ (solid line with open circles) and $M_{\text{cut}} = 7.56 M_{\odot}$ (dashed-dotted line with open circles). This model corresponds to the matter ejected in the equatorial plane of the primary where we assumed that the secondary star is located (for more details, see González Hernández et al. 2005b). Right panel: same as left panel but in this model we have assumed complete lateral mixing, where all the material within given velocity bins is completely mixed. Two simulations are shown for two different mass-cuts, $M_{\text{cut}} = 2.41 M_{\odot}$ (solid line with open circles) and $M_{\text{cut}} = 7.56 M_{\odot}$ (dashed-dotted line with open circles).

ement abundances can be reproduced for all mass-cuts. This means that neither substantial fallback nor an efficient mixing process is needed. For mass-cuts above $\sim 3 M_{\odot}$, very little Si, Ca, Ti, Fe, and Ni is ejected; thus, the expected abundances of the model essentially reflect the initial abundances of the secondary star. In contrast, Mg and Al are not sensitive to the mass-cut and are slightly enhanced due to the capture of enriched material in the SN explosion.

We also investigate a model with solar initial abundances for the secondary star, i.e., $[X/H]_0 = 0$, and the same explosion model of solar metallicity ($Z = 0.02$), which would fit all the element abundances if the mass-cut is low enough ($M_{\text{cut}} \lesssim 3 M_{\odot}$) and mixing is so efficient that significant amounts of elements which form in the inner layers of the explosion (such as Ti, Ni, and Fe) are present in the ejecta.

5.5. Non-Spherical Explosion: Formation in the Thin Disk

In this section, the thin-disk scenario is studied using non-spherically symmetric explosion models from Maeda et al. (2002). The chemical composition of the ejecta in a non-spherically symmetric SN explosion is strongly dependent on direction. In particular, if we assume that the jet is collimated perpendicular to the orbital plane of the binary, where the secondary star is located, elements such as Ti, Fe, and Ni are mainly ejected in the jet direction, while O, Mg, Al, Si, and S are preferentially ejected near the equatorial plane of the helium star (Maeda et al. 2002).

In Fig. 13 we compare the predicted abundances in the secondary star after pollution from an aspherical explosion model of a metal-rich progenitor having a $16 M_{\odot}$ He core (see also Table 6). The initial abundances of the secondary were extracted from the average values of stars of the solar neighborhood with

similar iron content (see Table 3). The left panel reflects the composition of the material ejected in the equatorial plane while in the right panel we have considered complete lateral mixing (Podsiadlowski et al. 2002) — that is, the ejected matter is completely mixed within each velocity bin. This mixing process is done with the decayed yields of the model, and after that, all the material above the mass-cut is mixed and used to calculate the composition of the ejected matter. The observed abundances are better reproduced if complete lateral mixing is considered since this process tends to enhance all of the element abundances at all mass-cuts. However, the equatorial model (left panel) also provides good fits to the observed abundances. It should be noted that in this model, only the material ejected in the equatorial plane is captured and therefore, only Mg, Al, and Si are significantly enhanced with respect to the initial abundances. A model with solar initial abundances for the secondary star, i.e. $[X/H]_0 = 0$, and the same explosion model of solar metallicity ($Z = 0.02$) was also inspected, providing the same result except for the equatorial model which produces too low abundances of Ti, Fe, and Ni in comparison with the observations.

Both aspherical explosion models with initial abundances equal to the average values of thin-disk stars show little dependence on the mass-cut, and since the equatorial model can reproduce the observed abundances, extensive mixing processes are not required. In addition, the non-spherically symmetric ejection of the mass in the explosion could provide the kick that the system needs to change its orbit from the Galactic plane to the current orbit. Therefore, the element abundances in the secondary star and the kinematics of this system strongly suggest that the binary system XTE J1118+480 formed in the Galactic disk (probably the thin disk) and it was then

kicked towards the Galactic halo, most probably by asymmetric mass ejection in an asymmetric supernova/hypernova explosion that gave rise to the black hole in this system.

The elements O and C, for which we provide the expected abundances in Tables 5 and 6, could be studied in future investigations, probably from CO and OH bands in the near-IR. This would help to recognize the operation of the CNO cycle on the surface the secondary star, proposed by Haswell et al. (2002), and possible processes of rotation-induced mixing during the evolution of the massive star.

6. Conclusions

We have presented Keck II/ESI medium-resolution spectroscopy of the black hole binary XTE J1118+480. The individual spectra of the system allowed us to derive an orbital period of $P = 0.16995 \pm 0.00012$ d and a radial velocity semiamplitude of the secondary star of $K_2 = 708.8 \pm 1.4$ km s⁻¹. The implied updated mass function is $f(M) = 6.27 \pm 0.04$ M_⊙, consistent with (but more precise than) previous values reported in the literature. Inspection of the high-quality averaged spectrum of the secondary star provides a rotational velocity of $v \sin i = 100^{+3}_{-11}$ km s⁻¹, and hence a binary mass ratio $q = 0.027 \pm 0.009$. The derived radial velocity, $\gamma = 2.7 \pm 1.1$ km s⁻¹, of the center of mass of the system agrees, at the 3σ level, with the results of previous studies.

We have performed a detailed chemical analysis of the secondary star. We applied a technique that provides a determination of the stellar parameters, taking into account any possible veiling from the accretion disk. We find $T_{\text{eff}} = 4700 \pm 100$ K, $\log[g/\text{cm s}^2] = 4.6 \pm 0.3$, $[\text{Fe}/\text{H}] = 0.18 \pm 0.17$, and a disk veiling (defined as $F_{\text{disk}}/F_{\text{total}}$) of $\sim 40\%$ at 5000 Å, decreasing toward longer wavelengths.

We have provided further details on the abundances of Mg, Al, Ca, Fe, Ni, and Li already reported by González Hernández et al. (2006), and we determined new element abundances of Si and Ti. The chemical abundances are typically higher than solar, and in some cases they are slightly enhanced (e.g., Mg, Al, and Si) in comparison with the abundances of these elements in stars of the solar neighborhood having similar iron content.

The present location and kinematics of this binary system had suggested that it could have originated in the Galactic halo. However, the chemical abundances strongly indicate that the black hole formed as a consequence of a supernova/hypernova explosion that occurred within the binary system. This explosive event must have either provided a kick to the system if it was formed in the thin disk or enriched significantly the atmosphere of the secondary star if the system formed in the thick disk or halo.

We have explored a variety of supernova/hypernova explosion models for different metallicities, He core masses, and geometries. We compared the expected abundances in the secondary star after contamination from nucleosynthetic products from different initial metallicities of the secondary star ($-2.2 < [\text{Fe}/\text{H}] < 0.2$), to investigate the formation region in the Galactic halo, thick disk, or thin disk. Metal-poor explosion models ($Z = 0$ and $Z = 0.001$) were not able to fit the observed abundances since they produce inappropriate ratios between α -elements and iron-peak elements, and they are extremely sensitive to the adopted mass-cut. This comparison probably rules out an origin in the Galactic halo for this black hole binary.

For the thick-disk scenario, we carefully inspected the model predictions, and although they provide better fits to the observed abundances, they require substantial fallback (up to $5.5 M_{\odot}$) and very efficient mixing processes

between the inner layer of the explosion and the ejecta. We thus conclude that this scenario is unlikely.

Metal-rich spherically symmetric models for the thin-disk scenario were able to fairly reproduce the observed abundances, although they do not easily provide the energy required to launch the system from the Galactic plane to its current halo orbit.

Finally, non-spherically symmetric models produce excellent agreement with the observed element abundances in the secondary star without invoking extensive fallback and mixing. In addition, asymmetric mass ejection would naturally provide the kick to expel this binary system from its birth place in the Galactic thin disk, which seems to be the most plausible explanation for the origin of this halo black hole X-ray binary.

We thank Keiichi Maeda for providing us with his aspherical explosion models, and for helpful discussions. We are grateful to Tom Marsh for the use of the MOLLY analysis package. The W. M. Keck Observatory is operated as a scientific partnership among the California Institute of Technology, the University of California, and NASA; it was made possible by the generous financial support of the W. M. Keck Foundation. This work has made use of the VALD database and IRAF facilities. J.I. acknowledges support from the EU contract MEXT-CT-2004-014265 (CIFIST). Additional funding was provided by Spanish Ministry project AYA2005-05149, as well as by US National Science Foundation grants AST-0307894 and AST-0607485 to A.V.F.

REFERENCES

- Allende Prieto, C., Barklem, P. S., Lambert, D. L., & Cunha, K. 2004, *A&A*, 420, 183
- Allende Prieto, C., et al. 2006, *ApJ*, 636, 804

- Al-Naimiy, H. M. 1978, *Ap&SS*, 420, 183
- Beer, M. E., & Podsiadlowski, Ph. 2002, *MNRAS*, 331, 351
- Bensby, T., Feltzing, S., Lundström, I., & Ilyin, I. 2003, *A&A*, 410, 527
- Bensby, T., Feltzing, S., Lundström, I., & Ilyin, I. 2005, *A&A*, 433, 185
- Benz, W., & Hills, J. G. 1992, *ApJ*, 433, 185
- Brunish, W. M., & Truran, J. W. 1982, *ApJS*, 49, 447
- Cayrel, R., et al. 2004, *A&A*, 416, 1117
- Chen, B. 1997, *ApJ*, 491, 181
- D’Antona, F., & Mazzitelli, I. 1994, *ApJS*, 90, 467
- Ecuvillon, A., Israelian, G., Santos, N. C., Mayor, M., Villar, V., & Bihain, G. 2004, *A&A*, 426, 619
- Ecuvillon, A., Israelian, G., Santos, N. C., Shchukina, N. G., Mayor, M., & Rebolo, R. 2006, *A&A*, 445, 633
- Frontera, F., et al. 2001, *ApJ*, 561, 1006
- Gelino, D. M., Harrison, T. E., & Orosz, J. A. 2001, *ApJ*, 122, 2668
- Gelino, D. M., Balman, Ş., Kililoğlu, Ü., Yilmaz, A., Kalemci, E., & Tomsick, J. A. 2006, *ApJ*, 642, 438
- Gilli, G., Israelian, G., Ecuvillon, A., Santos, N. C., & Mayor, M. 2006, *A&A*, 449, 723
- González Hernández, J. I., Rebolo, R., Israelian, G., Casares, J., Maeder, A., & Meynet, G. 2004, *ApJ*, 609, 988
- González Hernández, J. I., Rebolo, R., Israelian, G., Casares, J., Maeda, K., Bonifacio, P., & Molaro, P. 2005, *ApJ*, 630, 495
- González Hernández, J. I., Rebolo, R., Israelian, G., Harlaftis, E. T., Filippenko, A. V., & Chornock, R. 2006, *ApJ*, 644, L49
- Grevesse, N., Noels, A., & Sauval, A. J. 1996, in *Cosmic Abundances*, ed. S. S. Holt & G. Sonneborn (San Francisco: ASP, Conf. Ser. Vol. 99), 117
- Gualandris, A., Colpi, M., Portegies Zwart, S., & Possenti, A. 2005, *A&A*, 618, 845
- Haswell, C. A., Hynes, R. I., King, A. R., & Schenker, K. 2002, *MNRAS*, 332, 928
- Hills, J. G. 1983, *ApJ*, 267, 322
- Hills, J. G. 1991, *ApJ*, 102, 2
- Hynes, R. I., Robinson, E. L., & Bitner, M. 2005, *ApJ*, 630, 405
- Israelian, G., Rebolo, R., Basri, G., Casares, J., & Martín, E. L. 1999, *Nature*, 401, 142
- Jonsell, K., et al. 2005, *A&A*, 440, 321
- Kifonidis, K., Plewa, T., Janka, H.-Th., & Müller, E. 2000, *A&A*, 531, L123
- Kurucz, R. L. *ATLAS9 Stellar Atmospheres Programs and 2 km s⁻¹ Grid*. (CD-ROM, Smithsonian Astrophysical Observatory, Cambridge, 1993).
- Kurucz, R. L., Furenlid, I., Brault, J., & Testerman, L. 1984, *Solar Flux Atlas from 296 to 1300 nm*, *NOAO Atlas 1* (Cambridge: Harvard Univ. Press)
- Lai, D., Chernoff, D. F., & Cordes, J. M. 2001, *ApJ*, 549, 1111
- MacFadyen, A. I., Woosley, S. E., & Heger, A. 2001, *ApJ*, 550, 410
- Maeda, K., Nakamura, T., Nomoto, K., Mazali, P. A., Patat, F., & Hachisu, I. 2002, *ApJ*, 565, 405

- Marsh, T. R., Robinson, E. L., & Wood, J. H. 1994, MNRAS, 266, 137
- Martin, N. F., Ibata, R. A., Bellazzini, M., Irwin, M. J., Lewis, G. F., & Dehnen, W. 2004, MNRAS, 348, 12
- McClintock, J. E., Garcia, M. R., Caldwell, N., Falco, E. E., Garnavich, P. M., & Zhao, P. 2001, ApJ, 551, L147
- Mihalas, D., & Binney, J. 1981, Galactic Astronomy: Structure and Kinematics, 2nd ed. (New York: W. H. Freeman & Company)
- Mirabel, I. F., Dawan, V., Mignani, R. P., Rodrigues, I., & Guglielmetti, F. 2001, Nature, 413, 139
- Orosz, J. A., et al. 2001, ApJ, 555, 489
- Pavlenko, Ya. V., & Magazzù, A. 1996, A&A, 311, 961
- Piskunov, N. E., Kupka, F., Ryabchikova, T. A., Weiss, W. W., & Jeffery, C. S. 1995, A&AS, 112, 525
- Podsiadlowski, P., Nomoto, K., Maeda, K., Nakamura, T., Mazzali, P., & Schmidt, B. 2002, ApJ, 567, 491
- Portegies Zwart, S. M., Verbunt, F., & Ergma, E. 1997a, A&A, 321, 207
- Portegies Zwart, S. M. et al. 1997b, A&A, 328, 143
- Remillard, R., Morgan, E., Smith, D., & Smith, E. 2000, IAU Circ. No. 7389
- Reylé, C., & Robin, A. C. 2001, A&A, 373, 886
- Sadakane, K., et al. 2006, PASJ, 58, 595
- Sheinis, A. I., et al. 2002, A&A, 114, 851
- Snedden, C. 1973, PhD Dissertation, Univ. of Texas at Austin
- Tominaga, N., Umeda, H. & Nomoto, K. 2007, ApJ, 660, 516
- Torres, M. A. P., et al. 2004, ApJ, 612, 1026
- Umeda, H., & Nomoto, K. 2002, ApJ, 565, 385
- Umeda, H., & Nomoto, K. 2005, ApJ, 619, 427
- van den Heuvel, E. P. J., & Habets, G. M. H. J. 1984, Nature, 309, 598
- Wagner, R. M., et al. 2001, ApJ, 556, 42

This 2-column preprint was prepared with the AAS L^AT_EX macros v5.2.